ACS OMEGA

Open Access

http://pubs.acs.org/journal/acsodf

Article

Identification and Validation of B-Cell Epitopes on the VP1 Protein of Parvovirus B19 through Molecular Docking and Dynamics Simulation

Reuben Kuruvilla Thomas,◆ Ambritha Balasundaram,◆ Gracy Fathima, Sathish Sankar, Dicky John Davis G,* Mageshbabu Ramamoorthy, Nithiyanandan Saravanan, Swati Kumari, Sudhabharathi Reju, Ramya Barani, Sribal Selvarajan, Krishnasamy Kaveri, John Fletcher, Jason T. Blackard, George Priya Doss C, and Padma Srikanth

Cite This: https://doi.org/10.1021/acsomega.4c08353

Read Online

ACCESS | Metrics & More | Article Recommendations | Supporting Information

ABSTRACT: This study aimed to identify B-cell epitope candidates using multiple epitope identification software and *in silico* analysis of the modeled B19 V protein against specific antibodies using molecular docking and dynamics simulation. ***Materials and Methods***: Full-length amino acid sequences of the VP1 protein of B19 V were retrieved from NCBI. A consensus sequence was generated using CLC sequence viewer. Linear B cell epitopes were identified using Bepipred 2.0, ABCpred, and LBTope. The linear epitope was synthesized and validated against B19 V-specific antibodies. A 3D model of the B19 V VP1 consensus protein was generated using the ITASSER server. Discontinuous B cell epitopes were identified using Discotope 2.0 and Ellipro. Molecular docking and molecular dynamics simulation was performed to investigate the interaction between the modeled B19 V protein and specific anti-B19 V antibody. ***Results***: The identified epitope was 100% conserved and similarly identified through ABCpred and LBTope. The HADDOCK score and MDS analysis, such as hydrogen bond interactions and MMPBSA analysis, revealed that the VP1 and mAb H chains formed a significantly stable complex. The MDS demonstrated that the VP1-mAb H chain complexes had lower RMSF values around 130 to 200 residues, a region responsible for the catalytic network for enzyme activity; as a result, the flexibility of the antibody-bound VP1 decreased when compared to Apo-VP1. **Conclusion**: A viable epitope identified through this process was synthesized and validated using ELISA, which highlighted the role of the epitope identification process in diagnostics. This study also sheds light on the complex interplay between VP1 and the mAb H chain and highlights key binding specificity and stability determinants.

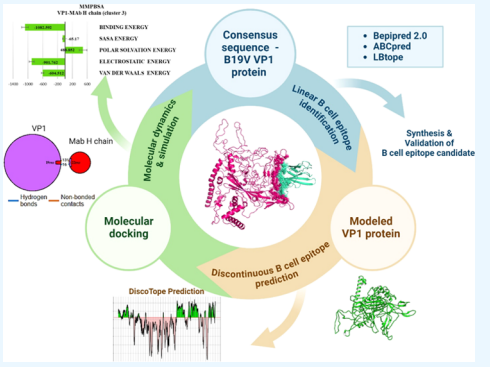

1. INTRODUCTION

Cossart et al. in 1975 discovered Human Parvovirus B19 (B19 V) during screening for hepatitis B virus.[1] B19 V is generally self-limiting but is harmful to high-risk individuals, including pregnant women, hematologically stressed individuals, and immunosuppressed people.[2,3] B19 V consists of a linear single-stranded DNA genome that is 5596 nucleotides long. The genome comprises two large open reading frames—an individual nonstructural protein (NS1) and two capsid proteins (VP1 and VP2).[4,5] The NS1 protein is 681 amino acids (aa) long with a molecular mass of 78 kDa. The minor capsid protein VP1 has a length of 781 amino acids and a molecular mass of 84 kDa, while the major capsid protein VP2 is 554 amino acids long and has a molecular mass of 58 kDa. The VP1 capsid protein located on the external surface of the virion is a dominant target for neutralizing antibodies.[6] Despite the prevalence of antibodies in the general population, instances of viremia are not as common.[7] The most reliable markers of acute B19 V infection involve the detection of IgM antibodies and a 4-fold increase or seroconversion of IgG levels in paired serum samples.[8] IgG antibodies persist for life and serve as markers of past infection.

The immune response against B19 V is directed against VP1 and VP2 proteins. Previous studies have documented multiple epitopes in the VP1u region and VP1/VP2.[9] Additionally, B19 V-specific cellular immunity develops against the B19 V VP1 and VP2 capsid proteins and the nonstructural protein (NS1).[10] The advancement in algorithms designed to identify suitable epitope candidates over the past decades has improved

Received: September 11, 2024
Revised: January 1, 2025
Accepted: January 9, 2025

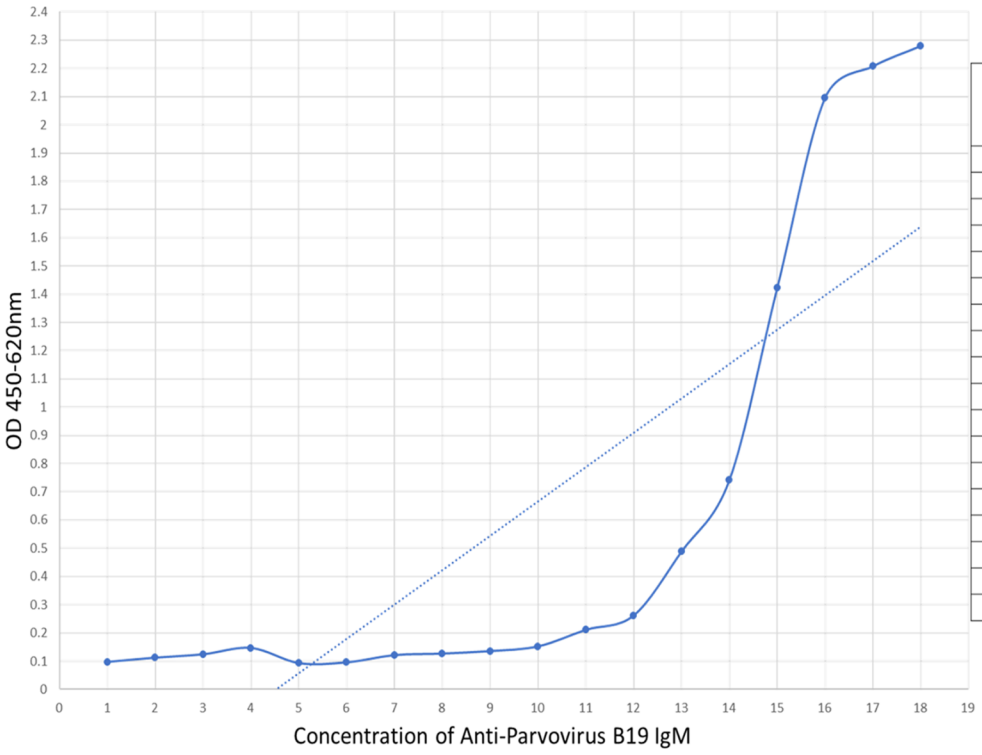

Sample		Mean	Standard Deviation
NC 2	1	0.096333	0.010214
NC 1	2	0.111333	0.008622
Blank 2	3	0.123333	0.047816
Blank 1	4	0.145667	0.015044
i/8192	5	0.092	0.002828
i/4096	6	0.094667	0.007572
i/2048	7	0.120333	0.023629
i/1024	8	0.125667	0.030238
i/512	9	0.134667	0.026764
i/256	10	0.151333	0.027025
i/128	11	0.21	0.020075
i/64	12	0.261	0.019925
i/32	13	0.487667	0.026026
i/16	14	0.740333	0.103254
i/8	15	1.422	0.022068
i/4	16	2.095667	0.056003
i/2	17	2.207667	0.035949
IgM	18	2.279667	0.032192

Figure 1. Plotted graph of synthesized B19 V epitope against Parvovirus B19 IgM (MyBioSource #MBS495442).

through in-depth computational analysis.[11] Progress in both B-cell epitope mapping and computational prediction has provided valuable molecular insights into the biorecognition process and the formation of antigen−antibody complexes.[12] These insights hold the potential to enhance the precise localization of B-cell epitopes.[13]

1.1. Importance. Molecular docking and dynamics simulation play a pivotal role in studying antigen−antibody interactions. Understanding these interactions has multiple applications, including vaccine development, antibody design, and development of diagnostic assays.[14] Traditional experimental methods, including X-ray crystallography and electron microscopy, are generally time-consuming and resource-intensive. Molecular docking to model the interaction between an antigen and an antibody is beneficial for identifying binding sites and predicting binding affinities. The primary goal of docking is to achieve an optimal fit between the antigen and the antibody that best simulates the *in vivo* binding process. The prediction of this binding provides the structural basis for understanding this interaction.[15] Protein−protein interaction is vital for the function of many biological molecules.[16,17] Protein−protein interactions are commonly studied using algorithms, such as HADDOCK, that use experimental data in the docking process. This approach helps understand the kinetics and thermodynamics of binding, the effects of solvent interactions, and the conformational changes that occur upon binding.[18,19] Molecular dynamics simulations (MDS) analyze binding interfaces and describe the conformational flexibility and stability that influence antigen−antibody binding.[20] Studies have demonstrated the role of MDS in identifying key residues and interaction patterns that affect the specificity and affinity of antibodies against antigens. Insights provided by MDS on the thermodynamics and kinetics of binding, binding free energy, and structural adaptations play a crucial role in the design of antigen-specific antibodies.[21]

Until recently, the role of B19 V in blood transfusion safety and its role in other comorbidities, including sickle cell anemia, chronic anemia, and transient aplastic crisis, has been overlooked. Our study has employed computational methods to identify and characterize B-cell epitopes of B19 V. A B-cell epitope deemed ideal based on the above computational methods was validated in the laboratory using ELISA. These computational approaches were instrumental in predicting the interaction between the identified epitopes and antibodies, providing a deeper understanding of the active sites of the modeled protein involved in the immune response against B19 V. This study aimed to identify B-cell epitope candidates using multiple epitope identification software and perform in-silico analysis of the modeled B19 V protein against B19 V-specific antibodies using molecular docking and molecular dynamics simulation.

2. MATERIALS AND METHODS

2.1. Consensus Sequence Identification. *2.1.1. Selection of Target Protein for Epitope Identification: B19 V VP1 Capsid Protein.* Neutralizing linear epitopes are concentrated in the VP1-unique and VP1-VP2 junction regions, eliciting a considerably more effective immune response than the VP2 region. Hence, in this study, the VP1 capsid protein of B19 V was selected as the target protein for epitope identification.

2.1.2. Sequence Retrieval and VP1 Consensus Sequence. A total of 996 sequences were retrieved from the NCBI database.[22] Of the 996 sequences, only full-length amino acid sequences of the VP1 protein of B19 V (n = 126) were selected. The VP1 sequences were aligned using CLC sequence viewer 8.0, generating a VP1 consensus sequence.

2.2. Linear B-Cell Epitope Identification. Linear B-cell epitopes were identified using Bepipred 2.0.[23] The proportion of the exposed and buried residues within each epitope identified was noted. Epitopes with a length between 15−30 aa

https://doi.org/10.1021/acsomega.4c08353
ACS Omega XXXX, XXX, XXX−XXX

that generated a score ((exposed/exposed + buried) × 100) of >70% were selected as viable epitopes. Epitope identification was similarly performed with ABCpred[24] and LBtope.[25] Default algorithm parameters were used for epitope identification. An epitope threshold of 0.5 was selected for epitope identification using Bepipred 2.0. A similar threshold of 0.51 with a default window length (16 amino acids) was used for epitope identification using ABCpred. For LBtope, the LBtope_Variable (original data set) was used, with a percent of probability of correct prediction more than 60% (default).

2.3. Synthesis and Validation of B-Cell Epitope Candidate. An ideal linear epitope candidate identified through Bepipred, ABCpred, and LBtope was synthesized and validated using an in-house ELISA (Figure 1). The epitope was initially tested against B19 V IgM antibody (MyBioSource #MBS495442) and NovaLisa B19 V IgM antibody (#PARM0370) (Supporting Figure 6). An indirect ELISA design was utilized in the validation of the epitope. The target of the ELISA was B19 V IgM antibodies. The secondary antibody used in the ELISA was an antihuman IgM (#ab99744 Mouse monoclonal [UHB] Anti-Human IgM mu chain (HRP-conjugated)). The solvent used in the dilution buffer, blocking buffer and wash buffer was 0.01 M Phosphate Buffer Saline (PBS) (pH 7.0). The blocking buffer was prepared with 3% Bovine Serum Albumin (BSA) in PBS. The wash buffer (PBST) constituted of PBS and 0.05% Tween-20.

The synthesized epitope was coated (5 μg/mL) on the microtiter plate and incubated at 4 °C overnight. Postwash, the wells were then blocked and the plate was incubated at 37 °C for 1 h. After a second wash, the target B19 V IgM antibodies were added and the plate was incubated at room temperature for 1 h. The plate was washed again, following which, the secondary antibody, HRP-conjugated mouse antihuman IgM was added and incubated at room temperature for 1 h. The chromogenic substrate, 3-3′-5-5′tetramethylbenzidine was added and the plate was incubated at room temperature for 30 min. After color change, stop solution was added and absorbance was measured at 450 and 620 nm. The testing was performed in triplicate and the mean and standard deviation were calculated. A calibration curve of the synthesized epitope against MyBioSource Parvovirus B19 IgM was generated. The synthesized B19 V epitope was also tested against NovaLisa Parvovirus B19 IgM antibodies (#PARM0370) using the same protocol.

2.4. Structure Prediction. The consensus sequence of the VP1 protein was input into an Iterative Threading ASSEmbly Refinement online server (I-TASSER).[26−28] Structural templates are initially identified from the protein databank (PDB) using the multiple threading approach, LOMETS. Iterative template-based fragment assembly simulations are used to generate full-length atomic models.

2.5. Structure Validation. For structural validation, the Ramachandran plot of the VP1 protein model was generated using the PROCHECK module from the SAVESv6.1 Web site (https://saves.mbi.ucla.edu/).

2.6. Discontinuous/Conformational B-Cell Epitope Prediction. Conformational B-cell epitopes were identified using Discotope 2.0[29] and Ellipro[30] in the predicted VP1 protein. The identified epitopes were labeled on the VP1 protein of B19 V using UCSF Chimera.[31]

2.7. Molecular Docking. Using the modeled structure of VP1, we simulated its interaction with a known neutralizing antibody, specifically the Fab region of the mAb H chain (PDB: 6NN3).[32] The binding affinity between the modeled VP1 protein and the mAb heavy chain Fab region (PDB ID: 6NN3_2) was investigated using the HADDOCK 2.4 (High Ambiguity-Driven protein−protein DOCKing) online server.[33] For this analysis, active sites on the VP1 protein—positions 284 to 303—were included. On the Fab region of the mAb heavy chain, the active sites considered were positions 26 to 33, 69 to 78, and 99 to 106. HADDOCK generates various docking conformations, which are then clustered based on their orientations. The cluster with the most members and the lowest Z-score is chosen as the final conformation since it indicates the most favorable and stable docking interaction. The PDBsum online server was utilized to identify the binding networks, including hydrogen bonds (H-bonds), salt bridges, and nonbonded contacts, between the VP1 protein and the mAb heavy chain.[34] These interactions were also visualized using PyMOL.[35] PRODIGY was used to predict the binding free energy (ΔG) and dissociation constant (K_d) of the best VP1-mAb H chain complexes derived from docking.[36] The intermolecular binding free energy of VP1 and the mAb H chain for Clusters 1 and 3 was evaluated using MMGBSA (Molecular Mechanics Generalized Born Surface Area) via the HawkDock web server to provide more critical insights than traditional scoring functions.[37]

2.8. Molecular Dynamics and Simulation (MDS). MDS was conducted to assess the motions and fluctuations of the Apo protein and the protein complexes (VP1-Mab H chain bound in Cluster 1 and Cluster 3). The initial stages of the protein complexes for MDS were obtained from docking studies, while the Apo protein was derived from the modeled structure. Molecular docking and simulation studies predict binding status in static conditions and under physiological environments, respectively. The structures were subsequently prepared for MDS using the GROMACS v.5.0.6 software package.[38] The AMBER99SB-ILDN force field was applied to generate the topology parameters of the structural complexes. The binary complexes were then placed in a cubic box filled with TIP3P water molecules. Before minimization, 15 sodium (Na^+) counterions were added to neutralize the system. Energy minimization was performed using the steepest descent algorithm for 50,000 steps to eliminate initial steric clashes. A 500 ps NVT (constant number of particles, volume, and temperature) equilibration was conducted at 300 K using a V-rescale thermostat. This was followed by a 500 ps NPT (constant number of particles, pressure, and temperature) equilibration at 1.0 bar. The systems were then subjected to a 10 ns production run under constant temperature (300 K) and pressure (1.0 bar). Long-range electrostatic interactions were calculated using the Particle Mesh Ewald (PME) method, and bond lengths were constrained using the LINCS algorithm.[39] The stability and behavior of the structural complexes during the MDS were monitored by calculating the Root Mean Square Deviation (RMSD) and Root Mean Square Fluctuation (RMSF) over the 200 ns simulation period. The radius of gyration (R_g), solvent-accessible surface area (SASA), and intermolecular H-bonds were calculated during the 200 ns simulation period to evaluate the protein complexes' compactness, structural stability, and interaction dynamics. The binding free energy was calculated using the MM/PBSA method with the g_mmpbsa tool in GROMACS.[40] Additionally, the dynamics of all systems were visualized and analyzed using the Visual Molecular Dynamics (VMD) program.[41]

https://doi.org/10.1021/acsomega.4c08353
ACS Omega XXXX, XXX, XXX−XXX

3. RESULTS

3.1. Consensus Sequence. A consensus sequence of the B19 V VP1 protein (781 amino acids) was generated (Supporting File 1).

3.2. Linear B Cell Epitope Identification. *3.2.1. Bepipred 2.0.* The consensus sequence of the VP1 protein of B19 V served as input into the Bepipred 2.0 server and generated 22 epitopes (Supporting Table 1). Of the 22 epitopes, four epitopes were selected with an exposed residue score of >70%. Of the four epitopes, **PAASSCHNASGKEAKVCT** (position 286 to 303) had 77.78% exposed residues and was selected as the ideal B cell epitope.

3.2.2. ABCpred −16 mer. The consensus sequence was similarly fed into ABCpred. By default, epitopes of 16 mer were identified. PAASSCHNASGKEAKV was recognized as a potential epitope using ABCpred, as the default permitted by ABCpred is 16aa. A list of all epitopes identified by ABCpred are listed in Supporting Table 2.

3.2.3. LBtope. The VP1 consensus sequence was input into LBtope, and epitopes with a length of 18 aa were identified. The exact epitope identified by Bepipred 2.0, **PAASSCH-NASGKEAKVCT**, with an SVM score of −0.61643557, was identified using LBTope. All epitopes identified by LBtope are listed in Supporting Table 3.

3.3. Validation of B-Cell Epitope Candidate. The above graph depicts the reactivity of the synthesized epitope against parvovirus B19 IgM antibody (#MBS495442).

3.4. Modeled VP1 Protein. The modeled protein had a C-score of −1.19, an estimated TM-score of 0.57 ± 0.15, and an estimated RMSD of 11.2 ± 4.6 Å. Five models, corresponding with the largest structure clusters, were deemed ideal models of the B19 V VP1 protein (clustered based on pairwise similarity). The modeled VP1 protein generated by ITASSER has been outlined in Supporting Figure 1. The PROCHECK module from the SAVESv6.1 Web site produced a Ramachandran plot of the VP1 protein model, which revealed that more than 90% of the amino acid residues are situated in the favored and allowed regions (Supporting Figure 2).

3.5. Discontinuous Epitopes. Multiple discontinuous epitopes were identified using Discotope 2.0 and Ellipro. The epitopes were highlighted on the modeled B19 V VP1 protein using UCSF Chimera and are available in Supporting Tables 4 and 5, Supporting Figures 3, 4, and 5.

3.5.1. Active Sites for Molecular Docking. The complex of the modeled B19 VP1 protein-6NN3 B19 V-specific antibody was visualized using UCSF Chimera.[21] (Figure 2)

3.6. Molecular Docking. The top clusters determined by the VP1 and mAb H chain's HADDOCK score led to the clusters' selection for further MDS (Table 1). We chose Cluster 3 and Cluster 1 based on their respective characteristics. Cluster 3 was selected due to its best overall HADDOCK score, lowest Z-score, and favorable interaction energies, making it the top candidate for a stable docking interaction. Cluster 1 was chosen for its largest cluster size, indicating it is the most representative conformation observed in the docking simulations. By selecting both clusters for MDS, we aim to explore the dynamics and stability of the most favorable interaction (Cluster 3) and the most statistically significant interaction (Cluster 1). This approach ensures a comprehensive understanding of the docking interactions between VP1 and the mAb H chain. The HADDOCK score of Cluster 3 demonstrated significantly preferred binding

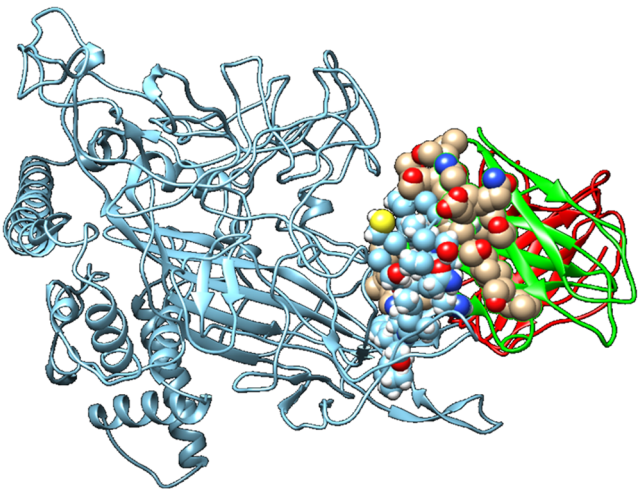

Figure 2. Visualization of interaction between modeled B19 V VP1 protein and Fab antibody (PDB id: 6NN3). Modeled B19 VP1 is illustrated in the blue cartoon structure, whereas Fab antibody H and L chains are displayed in green and red cartoon structures (sphere model). The interface residues between the B19 VP1 protein and Fab antibody are shown as spheres.

between VP1 and the mAb H chain (ΔG = −94.1 ± 3.3) compared to Cluster 1 (ΔG = −62.8 ± 2.7). This score indicates that Cluster 3 forms a more stable association with VP1 and the mAb H chain than Cluster 1. Analysis of the PDBsum database showed that the interface residues interact through both bonded and nonbonded interactions (Figure 3). The VP1-mAb H chain interface in Cluster 1 consists of 43 residues, with VP1 contributing 25 and the mAb H chain contributing 18. This cluster revealed 10 H-bonds and 125 nonbonded interactions (Figure 3A). Cluster 3 comprises 41 residues, with VP1 contributing 19 and the mAb H chain contributing 22. This cluster exhibited 16 H-bonds and 131 nonbonded interactions (Figure 3B). The binding affinity was measured using the docked complexes on the PRODIGY web server. Cluster 1 exhibited a stronger affinity (ΔG: −14.4 kcal/mol; Kd: 2.8×10^{-11} M) compared to Cluster 3 (ΔG: −13.4 kcal/mol; Kd: 1.5×10^{-10} M), both demonstrating significant interactions between VP1 and the MAb H chan. Furthermore, the binding free energies of the VP1-MAb H chain complexes were evaluated using HawkDock's MM/GBSA method. Cluster 1 had a binding free energy of −46.55 kcal/mol, while Cluster 3 exhibited a stronger affinity with a binding free energy of −58.96 kcal/mol.

3.6.1. Molecular Dynamics and Simulation (MDS). MDS of 200 ns were conducted for the Apo-VP1 protein and the VP1-mAb H chain Cluster 1 and Cluster 3 complexes. The generated trajectories were assessed for stability. The RMSD of the protein backbone was plotted to determine structural changes. The results indicated that the Apo-VP1 protein conformation stabilized at 8.10 nm after 60 ns, while the VP1-mAb H chain Cluster 1 and Cluster 3 complexes stabilized at 8.89 nm after 60 ns (Figure 4A).

The RMSF analysis is evaluated to understand the flexibility and stability of the protein regions. RMSF analysis shows that the average RMSF values for Apo-VP1 and the VP1-mAb H chain complexes (Cluster 1 and Cluster 3) are similar, ranging from 0.29 to 0.31 nm. However, a significant reduction in RMSF is observed around VP1 residues 130 to 200 upon Mab H chain binding, with RMSF decreasing to 0.6 nm compared

https://doi.org/10.1021/acsomega.4c08353
ACS Omega XXXX, XXX, XXX−XXX

Table 1. HADDOCK Docking Results for VP1-MAb H Chain

cluster	HADDOCK score	cluster size	RMSD from the overall lowest-energy structure	van der Waals energy	electrostatic energy	desolvation energy	restraints violation energy	buried surface area	*Z*-score
cluster 3*	−94.1 +/− 3.3	17	1.1 +/− 1.2	−61.6 +/− 2.8	−180.3 +/− 28.4	−13.2 +/− 5.8	168.1 +/− 38.0	2004.4 +/− 115.5	−2.1
cluster 2	−72.9 +/− 4.5	25	6.4 +/− 0.2	−56.7 +/− 4.8	−160.3 +/− 45.6	−7.0 +/− 3.5	229.0 +/− 47.8	1621.7 +/− 25.7	−0.7
cluster 6	−70.2 +/− 3.4	5	9.2 +/− 0.1	−55.0 +/− 3.8	−198.7 +/− 46.4	0.0 +/− 6.0	245.1 +/− 47.9	1927.2 +/− 76.0	−0.5
cluster 4	−66.0 +/− 2.5	12	3.9 +/− 0.2	−49.6 +/− 2.7	−136.8 +/− 19.2	−9.7 +/− 1.2	206.6 +/− 44.3	1671.3 +/− 57.3	−0.3
cluster 1*	−62.8 +/− 2.7	66	9.0 +/− 0.2	−51.9 +/− 12.3	−166.2 +/− 40.8	−0.8 +/− 2.0	231.6 +/− 53.0	1795.1 +/− 102.9	−0.1
cluster 9	−61.7 +/− 6.1	4	8.3 +/− 0.1	−48.4 +/− 3.2	−173.3 +/− 58.2	−4.1 +/− 2.6	254.4 +/− 78.8	1527.5 +/− 51.4	0
cluster 10	−61.0 +/− 8.1	4	8.5 +/− 0.0	−45.6 +/− 6.0	−167.5 +/− 14.9	−5.5 +/− 1.3	236.1 +/− 15.8	1683.5 +/− 88.8	0.1
cluster 5	−48.8 +/− 4.0	9	6.8 +/− 0.3	−43.2 +/− 0.9	−120.3 +/− 25.4	−6.8 +/− 1.7	251.8 +/− 54.0	1369.4 +/− 86.9	0.8
cluster 8	−48.1 +/− 6.0	4	7.7 +/− 0.1	−43.8 +/− 6.4	−72.7 +/− 25.5	−18.8 +/− 4.6	289.9 +/− 45.5	1308.1 +/− 108.2	0.9
cluster 7	−32.4 +/− 10.1	4	9.1 +/− 0.1	−37.8 +/− 5.6	−111.4 +/− 26.8	−3.5 +/− 4.0	311.9 +/− 43.1	1518.9 +/− 87.6	1.9

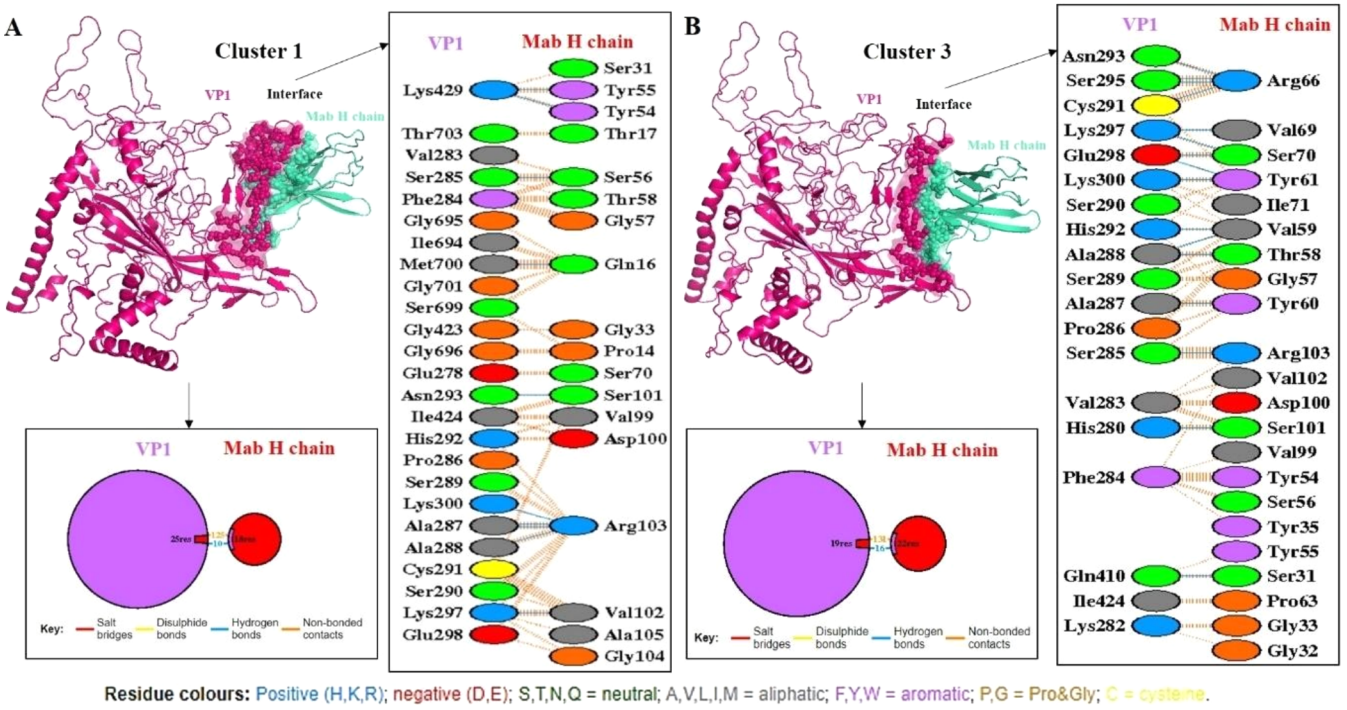

Figure 3. Molecular interactions between the VP1 and mAb H chain for Cluster 1 (A) and Cluster 3 (B) were illustrated using PyMOL and PDBsum.

to 1.2 nm in the apo form (Figure 4B). This reduction indicates that the binding stabilizes this region, restricting its movement and increasing its structural integrity.

The R_g analysis evaluates the overall compactness and structural stability of protein complexes. The average R_g value for Apo-VP1 is 2.98 nm. In contrast, the VP1-mAb H chain Cluster 1 and Cluster 3 complexes exhibit higher R_g values of 3.21 and 3.11 nm, respectively (Figure 4C). This increase suggests that Mab H chain binding induces a more extended conformation in VP1, resulting in a less compact structure and a broader spatial distribution of the protein's atoms.

The SASA values were studied to measure deviations in the surface of the protein structures. The SASA of Apo-VP1 was 415.03 nm^2, while the VP1-mAb H chain Cluster 1 and Cluster 3 complexes showed higher values of 466.75 and 477.08 nm^2, respectively (Figure 4D). This increase in SASA for the VP1-mAb H chain complexes suggests that the binding of the mAb H chain to VP1 exposes additional surface areas to the solvent. The slightly higher SASA in Cluster 3 than in Cluster 1 indicates that Cluster 3 may adopt a conformation that further increases the solvent-exposed surface area, most likely due to differences in the binding interface and interaction dynamics between VP1 and the mAb H chain.

Intermolecular H-bonds are crucial for maintaining the stability of complexes. To better understand the interaction between VP1 and the mAb H chain, the gmx Hbond program

https://doi.org/10.1021/acsomega.4c08353
ACS Omega XXXX, XXX, XXX−XXX

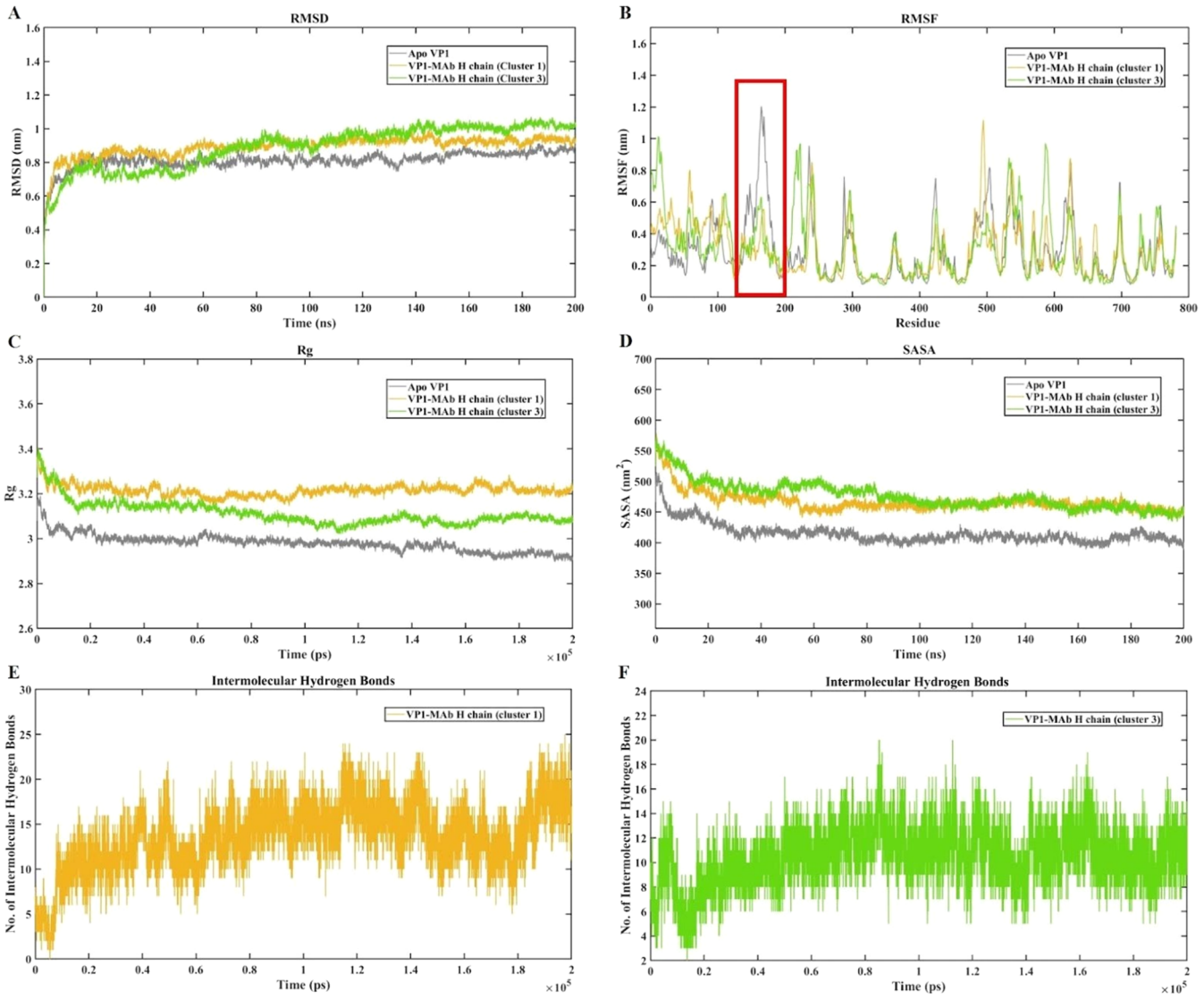

Figure 4. Plots for RMSD, RMSF, R_g, SASA, and intermolecular H-bonds were generated for the Apo-VP1, VP1-mAb H chain cluster 1, and VP1-mAb H chain cluster 3 complexes over 200 ns of MDS. (A) RMSD analysis of the backbone of the protein complexes Apo-VP1, VP1-mAb H chain cluster 1, and VP1-mAb H chain cluster 3. (B) RMSF analysis of the C-α atoms of the protein complexes Apo-VP1, VP1-mAb H chain cluster 1, and VP1-mAb H chain cluster 3. (C) R_g analysis for the complexes Apo-VP1, VP1-mAb H chain cluster 1, and VP1-mAb H chain cluster 3. (D) SASA analysis for the complexes Apo-VP1, VP1-mAb H chain cluster 1, and VP1-mAb H chain cluster 3. (E) Intermolecular hydrogen bond analysis between VP1 and mAb H chain in cluster 1. (F) Intermolecular hydrogen bond analysis between VP1 and mAb H chain in cluster 3.

was used to predict the number of H-bonds during the MDS. The number of H-bonds at the binding interface of both complexes remained essentially stable. Cluster 1 had an average of 13.57 H-bonds (with a maximum of 25), while Cluster 3 had an average of 10.48 H-bonds (with a maximum of 20) at the binding interface (Figure 4E,F).

MM/PBSA analysis is essential for estimating the free energy of binding between molecules in a complex, offering insights into their stability and interaction strength. For the VP1-mAb H chain complexes, Cluster 1 exhibits a binding energy of −898.642 ± 122.673 kJ/mol, with substantial contributions from van der Waals (−555.141 ± 43.905 kJ/mol) and electrostatic (−950.298 ± 117.310 kJ/mol) interactions (Table 2 and Figure 5A). In contrast, Cluster 3 demonstrates a stronger binding affinity with a binding energy of −1082.592 ± 90.098 kJ/mol, along with significant contributions from van der Waals (−604.512 ± 33.481 kJ/mol) and electrostatic (−901.762 ± 69.411 kJ/mol) interactions (Table 2 and Figure 5B). These results highlight significant interactions between VP1 and the mAb H chain in both clusters, with Cluster 3 showing a stronger binding affinity, as indicated by the more negative binding energy.

Table 2. MMPBSA Calculation of Binding Free Energies for VP1-MAb H Chain Cluster 1, and VP1-MAb H Chain Cluster 3 Complexes

	VP1-mAb H chain Cluster 1 (kJ/mol)	VP1-mAb H chain Cluster 3 (kJ/mol)
van der Waals energy	−555.141 +/− 43.905	−604.512 +/− 33.481
electrostatic energy	−950.298 +/− 117.310	−901.762 +/− 69.411
polar solvation energy	670.777 +/− 131.410	488.852 +/− 106.064
SASA energy	−63.979 +/− 4.556	−65.170 +/− 3.813
binding energy	−898.642 +/− 122.673	−1082.592 +/− 90.098

https://doi.org/10.1021/acsomega.4c08353
ACS Omega XXXX, XXX, XXX−XXX

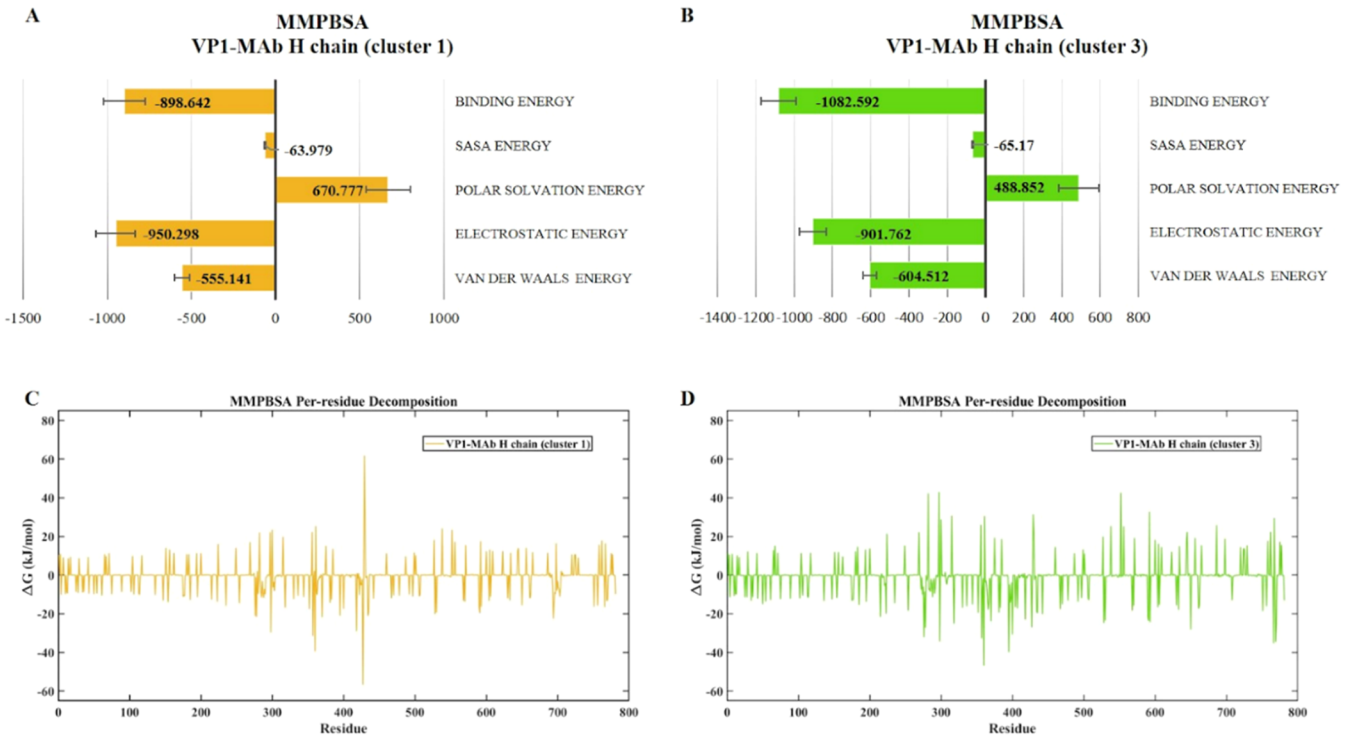

Figure 5. MMPBSA-calculated Energies Plot for the VP1-mAb H Chain Cluster 1 (A) and VP1-mAb H Chain Cluster 3 Complexes (B). The *x*-axis indicates the energy in kJ/mol. Additionally, residue decomposition MMPBSA plots illustrate the binding energy contribution of each residue for the VP1-mAb H chain cluster 1(C) and VP1-mAb H chain cluster 3 complexes (D).

Furthermore, per-residue decomposition breaks down the MM/PBSA energy to reveal the contribution of individual residues to the overall binding energy, identifying key residues involved in binding and aiding in targeted modifications. In cluster 1, higher binding energies were observed from residues 280 to 450 (Figure 5C). In cluster 3, significant contributions came from residues 280 to 450, 530 to 680, and 750 to 781 (Figure 5D). These findings revealed strong interactions between VP1 and the mAb H chain in both clusters, with Cluster 3 including a greater range of key residues implicated in binding.

During the MDS, the VP1 protein and mAb H chain residues were evaluated for unique H-bonds within a 3 Å distance to evaluate molecular interactions via VMD. Table 3 summarizes the unique H-bonds with more than 10% occupancy. The specific donor and acceptor residues and the percentage of simulation frames in which the H-bond was found are listed for each identified hydrogen bond. Cluster 1 of the VP1-mAb H chain formed 257 unique H-bonds, while Cluster 3 formed 232. Additionally, a heatmap was generated to visualize the count of H-bonds formed in each frame between unique residue pairs within a 5 Å distance (Figure 6). This visualization includes only those H-bonds with an occupancy above 10%, as detailed in Table 1. The heatmap provides a comprehensive view of the dynamic interactions between the VP1 protein and the mAb H chain throughout the simulation.

4. DISCUSSION

Multiple epitopes have been identified within the B19 V VP1 and VP2 proteins, and several studies have documented neutralizing epitopes in the VP1u region and the VP1-VP2 junction.[9,42,43] These epitopes generate a stronger response in comparison to the VP2 region. Neutralization epitopes on the VP1u region are primarily linear and were mapped at the N-terminal (80 aa position).[43] Studies have documented that B19 V-specific B-cell memory is directed against the conformational epitopes of VP2 and VP1 linear epitopes.[42] However, it is not directed against linear VP2 epitopes. Some studies have also documented immunoglobulin response against B19 V NS1. There are no reports about the immune response against the smaller 11.5 and 7.5 kDa nonstructural proteins despite expression of the 11.5 kDa protein at 100× that of NS1 during B19 V infection.[44,45] We chose VP1 as the target protein for epitope identification because of the clustering of the epitopes in the VP1u and VP1-VP2 region and their associated immunogenic response.

Based on previously published literature, we selected linear epitopes between 15 and 30 amino acids in length and have documented that this epitope length falls within the range of an ideal epitope.[25,29] The linear B-cell epitope **PAASSCH-NASGKEAKVCT** was 100% conserved and deemed the ideal B-cell epitope candidate. ABCpred and LBtope identified the same epitope. Model 1, generated by the ITASSER server, was selected as the best model due to the high score. A visualization of the modeled VP1 protein and the light and heavy chains of the Fab antibody (PDB id: 6NN3) was generated using CHIMERA to identify potential active sites on the modeled protein. The synthesized epitope is wholly located within the active region, as observed in Figure 2. The C-score is a confidence score employed by the I-TASSER server to determine the quality of predicted models. This score is derived from the significance of threading template alignments and the convergence parameters of structure assembly simulations. C-scores typically range from −5 to 2, with higher values indicating models of greater confidence.[27,28] TM-

https://doi.org/10.1021/acsomega.4c08353
ACS Omega XXXX, XXX, XXX−XXX

Table 3. Analysis of the MDS for the Most Occupied H-Bonds between VP1-MAb H Chain Clusters 1 and 3, Including Protein Residues and Occupancy Percentages

Donor	Acceptor	Occupancy (%)
VP1-mAb H chain (Cluster 1) − found 257 unique hydrogen bonds		
MAb_TYR54-Side−OH	VP1_SER285-Main-O	73.93
MAb_ARG103-Side-NH2	VP1_ ALA288-Main-O	27.45
VP1_SER290-Side-OG	MAb_SER101-Main-O	25.23
MAb_GLN76-Side-NE2	VP1_ ILE702-Main-O	22.48
MAb_ARG98-Side-NH1	VP1_ASP427-Side-OD1	20.26
MAb_ARG98-Side-NH2	VP1_ ASP427-Side-OD2	19.74
MAb_SER56-Side-OG	VP1_ PHE284-Main-O	17.69
MAb_GLY32-Main-N	VP1_GLN422-Side-OE1	17.01
MAb_THR17-Side-OG1	VP1_ASP360-Main-O	16.37
MAb_ARG98-Side-NH1	VP1_ASP427-Side-OD2	13.69
VP1_THR704-Side-OG1	MAb_ASP74-Side-OD2	13.31
MAb_ARG98-Side-NH2	VP1_ASP427-Side-OD1	12.78
MAb_GLY33-Main-N	VP1_ASP427-Side-OD1	12.34
VP1_THR704-Side-OG1	MAb_ASP74-Side-OD1	12.26
VP1_ILE702-Main-N	MAb_GLN76-Side-OE1	11.1
VP1-mAb H chain (Cluster 3) − found 232 unique hydrogen bonds		
MAb_TYR60-Side−OH	VP1_ASP395-Side-OD1	22.65
VP1_VAL283-Main-N	MAb_SER101-Main-O	22.25
MAb_ARG98-Side-NH1	VP1_GLU278-Side-OE1	19.39
MAb_ARG98-Side-NH2	VP1_GLU278-Side-OE2	19.03
MAb_SER28-Side-OG	VP1_ASP360-Side-OD1	17.4
MAb_ARG66-Side-NH2	VP1_GLU298-Side-OE2	16.02
MAb_ARG98-Side-NH1	VP1_GLU278-Side-OE2	15.98
MAb_ARG66-Side-NH1	VP1_GLU298-Side-OE1	15.71
MAb_ARG66-Side-NH1	VP1_GLU298-Side-OE2	15.5
MAb_ARG66-Side-NH2	VP1_GLU298-Side-OE1	15.48
MAb_ARG98-Side-NH2	VP1_GLU278-Side-OE1	15.05
VP1_TYR275-Main-N	MAb_SER31-Main-O	13.69
MAb_SER28-Side-OG	VP1_ASP360-Side-OD2	12.85
VP1_LEU397-Main-N	MAb_SER56-Main-O	11.97
VP1_LEU397-Main-N	MAb_THR58-Side-OG1	10.62

score and RMSD are well-documented metrics for evaluating structural similarity between two structures. When the native structure is known, they are used to determine the accuracy of structure modeling. However, it is essential to estimate the quality of the predicted model when the native structure is unknown. It estimates the distance between the predicted model and the native structure. The VP1 protein model shows strong structural integrity with 93.6% of residues in favored and allowed Ramachandran regions and a VERIFY 3D score of 77.08%, which is close to the 80% threshold and indicates a well-folded structure (Supporting Figure 7). As the protein size was larger (781 amino acids), little variations in trivial regions are acceptable and have no impact on the binding site, therefore being appropriate for docking experiments. It anticipates that small flaws can be stabilized by refinement using MDS, aligning the model with accepted criteria for flexible viral proteins. However, additional experimental validation, like X-ray crystallography, could improve confidence among structurally problematic regions.

BepiPred-2.0 uses a random forest model trained on structural data, primarily antigen−antibody complexes, which allows for the prediction of both linear and conformational epitopes with better accuracy.[23] It is reliant on multiple structural features such as hydrophobicity, polarity, and surface accessibility which improves its predictive power especially with conformational epitopes. With an AUC score of 0.62 on cross-validation data sets, BepiPred-2.0 demonstrates higher precision for high-scoring epitope predictions when compared against slightly older models such as LBtope. Random forest algorithms are excellent for handling complex data relationships, such as those found in conformational epitopes with noncontiguous residues, However, they can be computationally intensive, especially with large data sets and decision trees leading to longer processing time.

B-cell epitopes and nonepitope peptides from the Bcipep database (BCIPEP) were used to train the ABCpred algorithm. ABCpred uses a Recurrent Neural Network (RNN), specifically a Jordan network.[24] Its RNN is trained on linear epitopes, which are sequentially contiguous in the protein chain, ideal for identifying linear B-cell epitopes with fixed window lengths. ABCpred received an accuracy score of 66% in cross-validation tests, with moderate sensitivity and specificity scores. However, the window length feature of ABCpred is a limitation in the detection of longer epitopes. RNNs struggle with overfitting on small data sets and can be computationally demanding with sequential processing. LBtope is based on Support Vector Machine (SVM) and has been trained across multiple data sets, including fixed and

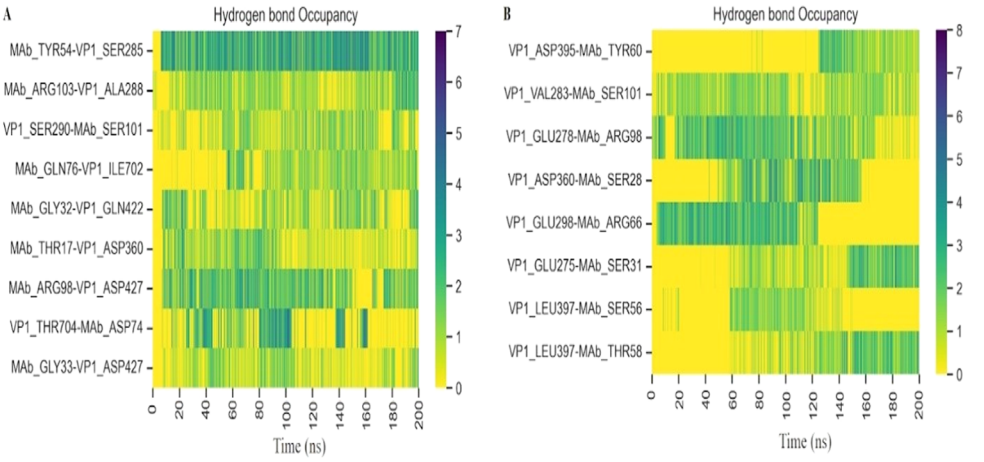

Figure 6. Hydrogen bond occupancy heatmap demonstrating dynamic interactions between VP1 Protein and mAb H Chain for Cluster 1 (A) and Cluster 3 (B) within 5 Å Distance.

https://doi.org/10.1021/acsomega.4c08353
ACS Omega XXXX, XXX, XXX−XXX

variable-length-B-cell epitopes from the Immune Epitope Database (IEDB).[25] It is ideal for the prediction of linear epitopes and has a sensitivity between 54 and 86%. It classifies epitopes and nonepitopes based on features such as dipeptide composition, and amino acid pair profiles. Both ABCpred and LBtope do not perform well in the identification of conformational epitopes. The strength of SVM is in its ability to handle high-dimensional data, working with complex feature sets extracted from linear epitope data sets. However, they struggle with complex or overlapping data points, such as those in conformational epitopes.

Following *in silico* epitope identification, the linear B-cell epitope was synthesized. An indirect ELISA was performed to test the epitope against a synthetic B19 V IgM antibody (#MBS495442), and a calibration curve was generated. Following validation of the epitope with the synthetic IgM antibodies, the epitope was validated again using the NovaLisa B19 V IgM antibody (#PARM0370). In most countries, there is currently no screening and diagnosing B19 V infection,[46] highlighting the need for a vaccine. There is currently no vaccine available for B19 V despite multiple attempts at developing a B19 V vaccine.[47,48] Predicted linear and conformational B-cell epitopes identified in this study could also serve toward the design of peptide vaccine candidates.

We took a comprehensive approach using computational docking, MDS, and energetic analyses to elucidate the binding dynamics between VP1 and the mAb H chain. The HADDOCK score is calculated based on factors such as van der Waals intermolecular energy, electrostatic intermolecular energy, desolvation energy, distance restraints energy, and buried surface area. In addition to the HADDOCK score, the Z-score represents the number of standard deviations a particular cluster deviates from the average score. Clusters with negative Z-scores are considered better representations of a good HADDOCK cluster. Our findings reveal distinct characteristics of two selected clusters, each representing a unique aspect of the VP1-mAb H chain interaction. Cluster 3, identified through favorable HADDOCK scores and strong binding affinities, demonstrated a more stable association with VP1 and the mAb H chain. MDS further supported this by showcasing stable RMSD values and reduced RMSF in critical regions upon mAb H chain binding, indicating enhanced structural stability.

Conversely, Cluster 1, chosen for its largest cluster size and statistical significance, exhibited slightly weaker binding affinity but engaged a broader range of critical residues in the interaction. Through MM/PBSA analysis and per-residue decomposition, we explained the energetic contributions of individual residues, highlighting key regions crucial for binding in both clusters. The comprehensive evaluation of unique H-bonds formed during simulations provided insights into dynamic interactions between VP1 and the mAb H chain, further validating the stability and specificity of the binding interface. Heatmap visualization of H-bond interactions within a 5 Å distance highlights vital residues in stabilizing the VP1-mAb complex and suggests potential sites for further investigation in therapeutic applications.

According to homology studies, a phospholipase A2 motif has been found in the amino acid sequence of the VP1 unique region, which spans positions 130 to 195. It is proposed that the amino acid residues at positions 153, 157, 168, and 195 form the catalytic network for the enzymatic activity. Residues 130, 132, 134, and 154 are suggested to be essential for binding to phospholipid environments, such as cellular membranes or membrane compartments, whereas residue 162 (Lys) is believed to be vital for binding calcium ions.[49] Our RMSF analysis showed reduced flexibility in mAb-H chain-bound VP1 complexes around the 130 to 200 residues compared to Apo-VP1. This finding suggests mAb binding will disturb the catalytic network for the enzymatic activity. These findings deepen our understanding of the VP1-mAb H chain interaction, offering valuable insights for rational design strategies to modulate or enhance this interaction for therapeutic or diagnostic purposes.

A limitation of this study is that we only focused on B cell epitopes and did not focus on T cell epitope identification and validation. However, based on the performed PDB blast, no structure for VP1 protein and additional B19 V-specific antibodies were available in the PDB database. There are only antibodies against the B19 V VP2 protein. The limited availability of the structures of B19 V-specific antibodies did not allow for further molecular docking and dynamics simulation.

5. CONCLUSIONS

In conclusion, this study highlighted a suitable epitope validated using an indirect ELISA and other epitopes that could further improve B19 V diagnostics. Our computational analysis is the first to detail the complex interaction between VP1 and the mAb H chain, unraveling key binding specificity and stability determinants. Through docking and MDS, we identified and characterized two distinct clusters representing stable and statistically significant VP1-mAb H chain interactions. Our results have emphasized the importance of considering structural stability and energetic contributions in evaluating VP1-mAb H chain interactions. This knowledge can guide future modifications or optimizations to improve the effectiveness of VP1-mAb H chain interactions in therapeutic development and diagnostic assays.

■ ASSOCIATED CONTENT

Data Availability Statement

All data generated from this study is available within the manuscript and Supporting Information.

Supporting Information

The Supporting Information is available free of charge at https://pubs.acs.org/doi/10.1021/acsomega.4c08353.

B19 V VP1 consensus sequence (File S1); B-cell epitopes that were identified by Bepipred 2.0 (Table S1); detailed epitopes that were identified using ABCpred and LBtope ranked according to their score (Tables S2 and S3); conformational B19 V epitopes that were identified using ElliPro (Table S4); Model 1 generated by the ITASSER Server (Figure S1), and the structural validation of the modeled B19 V VP1 protein using ProCheck (Figure S2); the prediction of B cell epitopes using Discotope 2.0. The green indicates areas of positive prediction while the red areas refer to areas of negative prediction. The conformational epitopes identified in Discotope 2.0 are highlighted in red using UCSF Chimera on the modeled B19 V VP1 protein (Figures S3 and S4); the modeled B19 V VP1 protein with conformational epitopes identified by ElliPro highlighted in orange using UCSF Chimera (Figure S5); calibration curve of the synthesized B19 V epitope

https://doi.org/10.1021/acsomega.4c08353
ACS Omega XXXX, XXX, XXX−XXX

against NovaLisa Parvovirus B19 IgM antibody (Figure S6); an analysis of model quality and credibility using Verify3D (Figure S7) (PDF)

AUTHOR INFORMATION

Corresponding Author

Dicky John Davis G − *Department of Bioinformatics, Sri Ramachandra Institute of Higher Education and Research, Chennai 600116 Tamil Nadu, India;* orcid.org/0000-0003-2325-7952; Email: dicky@sriramachandra.edu.in

Authors

Reuben Kuruvilla Thomas − *Department of Microbiology, Sri Ramachandra Institute of Higher Education and Research, Chennai 600116 Tamil Nadu, India;* orcid.org/0000-0001-5793-8911

Ambritha Balasundaram − *Department of Integrative Biology, School of Bio Sciences & Technology, VIT University, Vellore 632014 Tamil Nadu, India*

Gracy Fathima − *Department of Virology, King Institute of Preventive Medicine & Research, Chennai 600032 Tamil Nadu, India*

Sathish Sankar − *Department of Microbiology, Centre for Infectious Diseases, Saveetha Dental College and Hospitals, Saveetha Institute of Medical and Technical Sciences, Saveetha University, Chennai 600 077 Tamil Nadu, India;* orcid.org/0000-0002-9389-5231

Mageshbabu Ramamoorthy − *Sri Sakthi Amma Institute of Biomedical Research, Vellore 632055 Tamil Nadu, India*

Nithiyanandan Saravanan − *Sri Sakthi Amma Institute of Biomedical Research, Vellore 632055 Tamil Nadu, India*

Swati Kumari − *Department of Microbiology, Sri Ramachandra Institute of Higher Education and Research, Chennai 600116 Tamil Nadu, India*

Sudhabharathi Reju − *Department of Microbiology, Sri Ramachandra Institute of Higher Education and Research, Chennai 600116 Tamil Nadu, India*

Ramya Barani − *Department of Microbiology, Sri Ramachandra Institute of Higher Education and Research, Chennai 600116 Tamil Nadu, India*

Sribal Selvarajan − *Department of Microbiology, Sri Ramachandra Institute of Higher Education and Research, Chennai 600116 Tamil Nadu, India*

Krishnasamy Kaveri − *Department of Virology, King Institute of Preventive Medicine & Research, Chennai 600032 Tamil Nadu, India*

John Fletcher − *Department of Clinical Virology, Christian Medical College, Vellore 632004 Tamil Nadu, India*

Jason T. Blackard − *Department of Internal Medicine, Division of Digestive Diseases, University of Cincinnati, Cincinnati, Ohio 45267-0595, United States*

George Priya Doss C − *Department of Integrative Biology, School of Bio Sciences & Technology, VIT University, Vellore 632014 Tamil Nadu, India*

Padma Srikanth − *Department of Microbiology, Sri Ramachandra Institute of Higher Education and Research, Chennai 600116 Tamil Nadu, India*

Complete contact information is available at: https://pubs.acs.org/10.1021/acsomega.4c08353

Author Contributions

◆R.K.T. and A.B. have contributed equally to this manuscript. R.K.T., A.B., G.F., S.S., D.J.D.G., M.R., N.S., S.K., S.R., R.B., S.S., K.K., J.F., J.T.B., G.P.D.C., [1]*P.S. "Conceptualization, R.K.T., A.B., G.P.D. and P.S.; methodology, R.K.T., A.B., J.F.; software, R.K.T., A.B., G.P.D., M.R., N.S. D.J.; validation, R.K.T., A.B., S.K., R.B.; formal analysis, R.K.T., A.B., G.P.D., S.S., J.B., G.F., D.J.; investigation R.K.T., A.B., G.P.D., P.S., R.B.; resources P.S., G.P.D., G.F., S.S., M.R., K.K.; data curation R.K.T., A.B., G.P.D., J.B., S.S., J.F.; writing R.K.T., A.B.; writing—review and editing R.K.T., A.B., G.P.D., P.S., J.B., J.F., G.F., S.S.; visualization, R.K.T., A.B.; supervision G.P.D., P.S., S.S., M.R.; project administration, R.K.T., A.B., P.S.; funding acquisition, R.K.T., P.S. All authors have read and agreed to the published version of the manuscript.

Funding

Scheme for the Promotion of Academic and Research Collaboration, Ministry of Human Resource Development, Government of India (SPARC/2018−2019/P632/SL)

Notes

The authors declare no competing financial interest.

ACKNOWLEDGMENTS

This work was supported by the Scheme for the Promotion of Academic and Research Collaboration, Ministry of Human Resource Development, Government of India (SPARC/2018-2019/P632/SL). We would like to acknowledge the Merkoçi Nanobioelectronics and Biosensors Laboratory at the Institut Català de Nanociència i Nanotecnologia (ICN2), Barcelona, Spain, for their collaboration on the experimental work carried out in this study. We would also acknowledge the support from VIT management for the necessary facilities to perform the computational analysis.

REFERENCES

(1) Cossart, Y. E.; Field, A. M.; Cant, B.; Widdows, D. Parvovirus-like Particles in Human Sera. *Lancet* **1975**, *305* (7898), 72−73.

(2) Kishore, J.; Kishore, D. Clinical Impact & Pathogenic Mechanisms of Human Parvovirus B19: A Multiorgan Disease Inflictor Incognito. *Indian J. Med. Res.* **2018**, *148* (4), 373−384.

(3) Slavov, S. N.; Kashima, S.; Pinto, A. C. S.; Covas, D. T. Human Parvovirus B19: General Considerations and Impact on Patients with Sickle-Cell Disease and Thalassemia and on Blood Transfusions. *FEMS Immunol. Med. Microbiol.* **2011**, *62* (3), 247−262.

(4) Zhi, N.; Zádori, Z.; Brown, K. E.; Tijssen, P. Construction and Sequencing of an Infectious Clone of the Human Parvovirus B19. *Virology* **2004**, *318* (1), 142−152.

(5) Mori, J.; Beattie, P.; Melton, D. W.; Cohen, B. J.; Clewley, J. P. Structure and Mapping of the DNA of Human Parvovirus B19. *J. Gen. Virol.* **1987**, *68* (11), 2797−2806.

(6) Ozawa, K.; Young, N. Characterization of Capsid and Noncapsid Proteins of B19 Parvovirus Propagated in Human Erythroid Bone Marrow Cell Cultures. *J. Virol.* **1987**, *61* (8), 2627−2630.

(7) Marano, G.; Vaglio, S.; Pupella, S.; Facco, G.; Calizzani, G.; Candura, F.; Liumbruno, G. M.; Grazzini, G. Human Parvovirus B19 and Blood Product Safety: A Tale of Twenty Years of Improvements. *Blood Transfus.* **2015**, *13* (2), 184−196.

(8) Gallinella, G.; Zuffi, E.; Gentilomi, G.; Manaresi, E.; Venturoli, S.; Bonvicini, F.; Cricca, M.; Zerbini, M.; Musiani, M. Relevance of B19 Markers in Serum Samples for a Diagnosis of Parvovirus B19-Correlated Diseases. *J. Med. Virol.* **2003**, *71* (1), 135−139.

(9) Kurtzman, G. J.; Cohen, B. J.; Field, A. M.; Oseas, R.; Blaese, R. M.; Young, N. S. Immune Response to B19 Parvovirus and an Antibody Defect in Persistent Viral Infection. *J. Clin. Invest.* **1989**, *84* (4), 1114−1123.

(10) Saikawa, T.; Anderson, S.; Momoeda, M.; Kajigaya, S.; Young, N. S. Neutralizing Linear Epitopes of B19 Parvovirus Cluster in the VP1 Unique and VP1-VP2 Junction Regions. *J. Virol.* **1993**, *67* (6), 3004−3009.
(11) Backert, L.; Kohlbacher, O. Immunoinformatics and Epitope Prediction in the Age of Genomic Medicine. *Genome Med.* **2015**, *7* (1), No. 119.
(12) Hua, C. K.; Gacerez, A. T.; Sentman, C. L.; Ackerman, M. E.; Choi, Y.; Bailey-Kellogg, C. Computationally-Driven Identification of Antibody Epitopes. *eLife* **2017**, *6*, No. e29023.
(13) Potocnakova, L.; Bhide, M.; Pulzova, L. B. An Introduction to B-Cell Epitope Mapping and In Silico Epitope Prediction. *J. Immunol. Res.* **2016**, *2016*, No. 6760830.
(14) Guarra, F.; Colombo, G. Computational Methods in Immunology and Vaccinology: Design and Development of Antibodies and Immunogens. *J. Chem. Theory Comput.* **2023**, *19* (16), 5315−5333.
(15) Vakser, I. A. Protein-Protein Docking: From Interaction to Interactome. *Biophys. J.* **2014**, *107* (8), 1785−1793.
(16) Ali, Z.; Cardoza, J. V.; Basak, S.; Narsaria, U.; Singh, V. P.; Isaac, S. P.; França, T. C. C.; LaPlante, S. R.; George, S. S. Computational Design of Candidate Multi-Epitope Vaccine against SARS-CoV-2 Targeting Structural (S and N) and Non-Structural (NSP3 and NSP12) Proteins. *J. Biomol. Struct. Dyn.* **2023**, *41* (22), 13348−13367.
(17) Elshafei, S. O.; Mahmoud, N. A.; Almofti, Y. A. Immunoinformatics, Molecular Docking and Dynamics Simulation Approaches Unveil a Multi Epitope-Based Potent Peptide Vaccine Candidate against Avian Leukosis Virus. *Sci. Rep.* **2024**, *14* (1), No. 2870.
(18) Ambrosetti, F.; Jimenez-Garcia, B.; Roel-Touris, J.; Bonvin, A. M. J. J. Modeling Antibody-Antigen Complexes by Information-Driven Docking. *Structure* **2020**, *28*, 119−129.
(19) Sousa, S. F.; Fernandes, P. A.; Ramos, M. J. Protein−Ligand Docking: Current Status and Future Challenges. *Proteins:Struct., Funct., Bioinf.* **2006**, *65* (1), 15−26.
(20) Shaw, D. E.; Maragakis, P.; Lindorff-Larsen, K.; Piana, S.; Dror, R. O.; Eastwood, M. P.; Bank, J. A.; Jumper, J. M.; Salmon, J. K.; Shan, Y.; Wriggers, W. Atomic-Level Characterization of the Structural Dynamics of Proteins. *Science* **2010**, *330* (6002), 341−346.
(21) Sirin, S.; Apgar, J. R.; Bennett, E. M.; Keating, A. E. AB-Bind: Antibody Binding Mutational Database for Computational Affinity Predictions. *Protein Sci.* **2016**, *25* (2), 393−409.
(22) National Library of Medicine (NLM). Home - Nucleotide - NCBI. https://www.ncbi.nlm.nih.gov/nucleotide/. (accessed June 29, 2024).
(23) Jespersen, M. C.; Peters, B.; Nielsen, M.; Marcatili, P. BepiPred-2.0: Improving Sequence-Based B-Cell Epitope Prediction Using Conformational Epitopes. *Nucleic Acids Res.* **2017**, *45*, W24−W29, DOI: 10.1093/nar/gkx346.
(24) Saha, S.; Raghava, G. P. S. Prediction of Continuous B-Cell Epitopes in an Antigen Using Recurrent Neural Network. *Proteins:Struct., Funct., Bioinf.* **2006**, *65* (1), 40−48.
(25) Singh, H.; Ansari, H. R.; Raghava, G. P. S. Improved Method for Linear B-Cell Epitope Prediction Using Antigen's Primary Sequence *PloS one*, *8* e62216 DOI: 10.1371/journal.pone.0062216.
(26) Roy, A.; Kucukural, A.; Zhang, Y. I-TASSER: A Unified Platform for Automated Protein Structure and Function Prediction. *Nat. Protoc.* **2010**, *5* (4), 725−738.
(27) Yang, J.; Yan, R.; Roy, A.; Xu, D.; Poisson, J.; Zhang, Y. The I-TASSER Suite: Protein Structure and Function Prediction. *Nat. Methods* **2015**, *12* (1), 7−8.
(28) Zhang, Y. I-TASSER server for protein 3D structure prediction | BMC Bioinformatics | Full Text. https://bmcbioinformatics.biomedcentral.com/articles/10.1186/1471-2105-9-40. (accessed June 21, 2024).
(29) Kringelum, J. V.; Lundegaard, C.; Lund, O.; Nielsen, M. Reliable B Cell Epitope Predictions: Impacts of Method Development and Improved Benchmarking. *PLoS Comput. Biol.* **2012**, *8*, No. e1002829, DOI: 10.1371/journal.pcbi.1002829.
(30) Ponomarenko, J.; Bui, H.-H.; Li, W.; Fusseder, N.; Bourne, P. E.; Sette, A.; Peters, B. ElliPro: A New Structure-Based Tool for the Prediction of Antibody Epitopes. *BMC Bioinf.* **2008**, *9* (1), No. 514.
(31) Pettersen, E. F.; Goddard, T. D.; Huang, C. C.; Couch, G. S.; Greenblatt, D. M.; Meng, E. C.; Ferrin, T. E. UCSF Chimera—A Visualization System for Exploratory Research and Analysis. *J. Comput. Chem.* **2004**, *25* (13), 1605−1612.
(32) Sun, Y.; Klose, T.; Liu, Y.; Modrow, S.; Rossmann, M. G. Structure of Parvovirus B19 Decorated by Fabs from a Human Antibody. *J. Virol.* **2019**, *93* (9), No. 10-1128.
(33) Dominguez, C.; Boelens, R.; Bonvin, A. M. J. J. HADDOCK: A Protein−Protein Docking Approach Based on Biochemical or Biophysical Information. *J. Am. Chem. Soc.* **2003**, *125* (7), 1731−1737.
(34) Laskowski, R. A.; Jabłońska, J.; Pravda, L.; Vařeková, R. S.; Thornton, J. M. PDBsum: Structural Summaries of PDB Entries. *Protein Sci.* **2018**, *27* (1), 129−134.
(35) Lill, M. A.; Danielson, M. L. Computer-Aided Drug Design Platform Using PyMOL. *J. Comput.-Aided Mol. Des.* **2011**, *25* (1), 13−19.
(36) Xue, L. C.; Rodrigues, J. P.; Kastritis, P. L.; Bonvin, A. M.; Vangone, A. PRODIGY: A Web Server for Predicting the Binding Affinity of Protein−Protein Complexes. *Bioinformatics* **2016**, *32* (23), 3676−3678.
(37) Weng, G.; Wang, E.; Wang, Z.; Liu, H.; Zhu, F.; Li, D.; Hou, T. HawkDock: A Web Server to Predict and Analyze the Protein−Protein Complex Based on Computational Docking and MM/GBSA. *Nucleic Acids Res.* **2019**, *47* (W1), W322−W330.
(38) Abraham, M. J.; Murtola, T.; Schulz, R.; Páll, S.; Smith, J. C.; Hess, B.; Lindahl, E. GROMACS: High Performance Molecular Simulations through Multi-Level Parallelism from Laptops to Supercomputers. *SoftwareX* **2015**, *1−2*, 19−25.
(39) Hess, B.; Bekker, H.; Berendsen, H. J. C.; Fraaije, J. G. E. M. LINCS: A Linear Constraint Solver for Molecular Simulations. *J. Comput. Chem.* **1997**, *18* (12), 1463−1472.
(40) Kumari, R.; Kumar, R. Open Source Drug Discovery Consortium; Lynn, A. G_mmpbsa—A GROMACS Tool for High-Throughput MM-PBSA Calculations | Journal of Chemical Information and Modeling. 2014 https://pubs.acs.org/doi/10.1021/ci500020m. (accessed June 21, 2024).
(41) Humphrey, W.; Dalke, A.; Schulten, K. VMD: Visual Molecular Dynamics. *J. Mol. Graphics* **1996**, *14* (1), 33−38.
(42) Corcoran, A.; Mahon, B. P.; Doyle, S. B Cell Memory Is Directed toward Conformational Epitopes of Parvovirus B19 Capsid Proteins and the Unique Region of VP1. *J. Infect. Dis.* **2004**, *189* (10), 1873−1880.
(43) Ros, C.; Bieri, J.; Leisi, R. The VP1u of Human Parvovirus B19: A Multifunctional Capsid Protein with Biotechnological Applications. *Viruses* **2020**, *12* (12), No. 1463.
(44) Ennis, O.; Corcoran, A.; Kavanagh, K.; Mahon, B. P.; Doyle, S. Baculovirus Expression of Parvovirus B19 (B19V) NS1: Utility in Confirming Recent Infection. *J. Clin. Virol.* **2001**, *22* (1), 55−60.
(45) von Poblotzki, A.; Gigler, A.; Lang, B.; Wolf, H.; Modrow, S. Antibodies to Parvovirus B19 NS-1 Protein in Infected Individuals. *J. Gen. Virol.* **1995**, *76* (3), 519−527.
(46) Jia, J.; Zhang, M.; Ma, Y.; Zhang, J. Human Parvovirus B19 Research Concerning the Safety of Blood and Plasma Derivatives in China. *Ann. Blood* **2019**, *4* .
(47) Vuković, V.; Patić, A.; Ristić, M.; Kovačević, G.; Cvjetković, I. H.; Petrović, V. Seroepidemiology of Human Parvovirus B19 Infection among the Population of Vojvodina, Serbia, over a 16-Year Period (2008−2023). *Viruses* **2024**, *16* (2), No. 180.
(48) Mossong, J.; Hens, N.; Friederichs, V.; Davidkin, I.; Broman, M.; Litwinska, B.; Siennicka, J.; Trzcinska, A.; Van Damme, P.; Beutels, P.; Vyse, A.; Shkedy, Z.; Aerts, M.; Massari, M.; Gabutti, G. Parvovirus B19 Infection in Five European Countries: Seroepidemi-

https://doi.org/10.1021/acsomega.4c08353
ACS Omega XXXX, XXX, XXX−XXX

ology, Force of Infection and Maternal Risk of Infection. *Epidemiol. Infect.* **2008**, *136* (8), 1059−1068.
(49) Dorsch, S.; Liebisch, G.; Kaufmann, B.; von Landenberg, P.; Hoffmann, J. H.; Drobnik, W.; Modrow, S. The VP1 Unique Region of Parvovirus B19 and Its Constituent Phospholipase A2-Like Activity. *J. Virol.* **2002**, *76* (4), 2014−2018.

https://doi.org/10.1021/acsomega.4c08353
ACS Omega XXXX, XXX, XXX−XXX